EURASIP Journal on Wireless Communications and Networking

RESEARCH Open Access

3D target location based on RFID polarization phase model

Wei Shi[1], Zuhao Chen[1], Kun Zhao[1*], Wei Xi[1], Yuhang Qu[1], Hui He[1], Zhenge Guo[1], Zhe Ma[2], Xuhui Huang[2], Peng Wang[2], Bo Dong[2] and Jizhong Zhao[1]

*Correspondence: pandazhao1982@gmail.com
[1] School of Computer Science and Technology, Xi'an Jiaotong University, Xi'an, China
Full list of author information is available at the end of the article

Abstract

The three-dimensional target position is vital to automatic driving, which can efficiently detect the geometrical shape of obstacles and achieve automatic environment recognition for both indoor and outdoor scenarios. In this paper, we propose an RFID 3D localization prototype based on the polarization phase model. To eliminate the impacts of tag angle, we leverage the polarization effect to obtain polarized phases. After that, we use polarized phase decomposition to get pure phases, i.e., the phase corresponding to the line of sight path. Hence, we can calculate the raw phases using the HMFCW algorithm. Finally, we can estimate the target's 3D position according to unwrapped phase information. In this way, we implement a low-cost, high-precision, easy-for-deployment 3D position solution using commercial UHF RFID hardware. The experiments show that the method can obtain effective positioning results in various environments and achieve positioning accuracy with an average error of about 9 cm.

Keywords: 3D target localization, RFID, Polarization phase, Automatic driving

1 Introduction

Acquiring the object's position in three-dimensional physical space becomes an emergent demand in recent years. This is a fundamental service for industrial IoT APIs [1], smart home care [2], VANETs management [3], mobile context sensing [4] and real-time cloud scheduling [5]. As one of the most popular wireless positioning technology, RFID positioning technology mainly uses the RFID RF wave to detect the position of the target. With the rapid development of mobile computing devices, the demand for indoor positioning is increased. It is urgent to solve the problem of multitarget positioning in indoor scenes. Whether using GPS system [6] or mobile communication network based on Wi-Fi [7] or 5G [8, 9] for positioning, there are problems such as unstable active signal and strong environmental noise interference, which leads to a serious shortage of positioning accuracy and cannot meet the accuracy requirements of indoor positioning. Other approaches will introduce specialized equipment to the scenes, like ultra-wide band (UWB) [10], ultrasonic sensors [11, 12] and so on. Therefore, location based on RFID has become a hot research direction. Compared with other methods, the most prominent advantage of the positioning method based on RFID technology is that it can

make a relatively good positioning effect at a low cost. It can transform the positioning of objects into the positioning of tags, simplify the theoretical complexity of positioning and improve the positioning efficiency.

In view of the wide application prospect and implementation value of indoor positioning, especially three-dimensional positioning technology, this paper proposes a low-cost, convenient and efficient three-dimensional positioning method. Based on the existing commercial RFID equipment, by constructing the phase model based on polarization effect and combined with the signal propagation model in space, this paper proposes a three-dimensional positioning method based on pure signal extraction to achieve low cost. Highly reliable Indoor 3D positioning method.

The main work of this paper is based on RFID in three-dimensional space. The main problems and solutions are as follows: First, for the problems of high cost and difficult popularization in current positioning, it is necessary to use low-cost and large-scale deployable RFID tags as a substitute for target positioning to bind with the target object. Considering that the information that RFID tag can receive includes received signal strength, phase, timestamp and Doppler frequency shift, and the phase data have the highest accuracy, phase information is used as the basic parameter of positioning. Secondly, the problem of phase folding should be solved first when using phase for positioning. Because the phase changes periodically, the phase in a cycle can only be used to locate objects within more than ten centimeters, and the positioning range is too small. Therefore, HMFCW algorithm needs to be used to unwrap to improve the range of phase positioning. Thirdly, the phase information from the tag received by the reader receiving antenna contains not only the tag information, but the result of reflection superposition of multiple paths in space. Therefore, it is necessary to separate the pure phase information from the mixed information. Finally, because the existing phase models cannot describe the impact of label angle on phase, and label angle does affect phase in actual experiments, it is necessary to reconstruct the phase model related to label angle to ensure the accuracy of the phase model. The method proposed in this paper is mainly divided into the following two steps:

(1) Theoretical phase modeling: obtain the phase information of the tag to be tested from the existing commercial reader equipment, establish a polarization-based phase model for the tag phase and preprocess the phase with deconvolution and discrete wavelet transform denoising;

(2) Using phase positioning: decompose the phase on the basis of (1), extract the pure phase of the decomposed phase, eliminate the complex multipath information from the measured phase, use HMFCW algorithm to unwrap the phase, and finally, complete the positioning.

The main part of this paper is the process of reshaping the theoretical model according to the experiment. The first part is the modeling part, that is, the phase model based on the polarization effect. According to the experimental phenomena obtained in the experiment, it is found that the label angle has a great impact on the phase, but this is not mentioned in the existing phase model, therefore, based on the existing phase model, a phase model based on polarization effect is proposed, and the influence of label angle on phase is explained in detail. The second part is the positioning part. According to the theoretical model proposed above, it is found in the actual experiment that the

phase information provided by the existing commercial RFID equipment cannot directly match the theoretical model. The existence of multiple reflectors in the environment has a great impact on the experimental results, that is, the multipath effect. Therefore, this paper proposes a positioning algorithm based on pure phase extraction. Aiming at the multipath information in complex environments, this paper theoretically analyzes the relationship between pure phase and multipath phase, uses the collected phase information of different frequencies to fit the theoretical phase and corrects the error to ensure the accuracy of the pure phase. Finally, the pure phase at different frequencies is unwrapped to locate the label.

This paper designs a large number of experiments, modifies the theoretical model through the actual collected experimental data and designs a series of algorithms to reduce noise and error as much as possible. Finally, the feasibility of the algorithm is verified by experiments. Compared with the existing work, the research innovations and contributions of this paper are as follows:

(1) By analyzing the phenomenon of signal propagation and polarization in RFID system, a phase model based on the polarization effect is proposed, which accurately reflects the influence of tag angle on phase.
(2) By analyzing the theoretical relationship between actual phase information, pure phase and multipath phase, a positioning algorithm based on pure phase extraction is proposed, which eliminates the multipath phase from the phase obtained by commercial RFID readers, and solves the problem of the significant error increase of traditional positioning methods in multipath environment.
(3) There is no need to refer to labels or anchor points, and there is no need to collect a large number of training data, which improves the convenience of system deployment.
(4) Using commercial RFID equipment, a three-dimensional positioning algorithm with easy deployment, high precision and low cost is realized, and the average positioning error is about 9 cm.

2 System model based on polarization effect

In the previous section, we briefly introduce our basic idea and contribution. And then, we will describe the polarization effect and the phase model based on this effect.

In order to solve the influence of label angle on phase ignored in the existing phase model, a phase model based on polarization effect is proposed in this paper.

Because different label directions lead to different phases, the existing phase model cannot accurately quantify the relationship between phase and distance, and the fundamental reason for this phenomenon is polarization effect.

In order to explain the influence of tag direction on phase, this paper theoretically analyzes the signal propagation model of RFID. There can be a circular polarization between two antennas $\pi/2$ phase difference. If the directions of two orthogonal linear polarization antennas are marked as sum and the polarization direction of the label is marked as, the signal sent by the transmitting antenna is u, v and w:

$$S(t) = u\cos(kt) + v\cos\left(kt - \frac{\pi}{2}\right) = u\cos(kt) + v\sin(kt). \tag{1}$$

When the transmitted signal reaches the tag through propagation, the signal received at the tag end $S'(t)$ is

$$\begin{aligned} &S'(t) = S(t - t_d) = u\cos(kt - \theta_d) + v\sin(kt - \theta_d) \\ &\theta_d = 2\pi d/\lambda \end{aligned} \tag{2}$$

where t_d is the signal propagation time/s.

After the transmitted signal is printed on the tag, the tag collects energy, activates the working circuit and modulates its own information and polarization direction on the received signal, and the modulated received signal $S'(t)$ is

$$S''(t) = (u \cdot w)\cos(kt - \theta_d + \theta_t) + (v \cdot w)\sin(kt - \theta_d + \theta_t) \tag{3}$$

where θ_t is the phase offset/rad caused by hardware defect of tag.

After modulating the information, the tag will backscatter the signal into space. After the receiving antenna captures the signal of the tag in space, it can be decomposed into linear polarization components in two orthogonal directions. The signal decomposed by the receiving antenna in each direction vector is:

$$\begin{cases} S_u(t) = (u \cdot w)^2\cos(kt - 2\theta_d + \theta_t) + (u \cdot w)(v \cdot w)\sin(kt - 2\theta_d + \theta_t) \\ S_v(t) = (u \cdot w)(v \cdot w)\cos(kt - 2\theta_d + \theta_t) + (v \cdot w)^2\sin(kt - 2\theta_d + \theta_t) \end{cases} \tag{4}$$

The signal of the receiving antenna received by the reader is the superposition of the signals of the two linearly polarized antennas. Since the circularly polarized antenna is abstracted into two phases, the phase difference is $\pi/2$. The line polarized antenna, therefore, actually receives the signal can be $R(t)$ written as:

$$\begin{cases} R(t) = S_u(t) + S_v(t - \Delta t) = \cos(kt - 2\theta_d - \theta_t - \theta_r - \theta_o) \\ \tan\theta_o = \dfrac{2(u \cdot w)(v \cdot w)}{(u \cdot w)^2 - (v \cdot w)^2} \end{cases} \tag{5}$$

where θ_t is the phase offset/rad due to tag antenna hardware and θ_r is the phase offset/rad due to reader antenna hardware.

Equation (5) describes the influence of the label angle on the signal in the actual received signal, and the phase model based on polarization effect can be obtained

$$\begin{cases} \theta = \left(\dfrac{2\pi}{\lambda} \times 2d + \delta\right) mod 2\pi \\ \delta = \theta_o + \theta_t + \theta_r \\ \tan\theta_o = \dfrac{2(u \cdot w)(v \cdot w)}{(u \cdot w)^2 - (v \cdot w)^2} \end{cases} \tag{6}$$

where λ is the wavelength of electromagnetic wave/M; d is distance from antenna to tag/M; u, v are unit direction vectors of reader antenna; w is the unit direction vector of the label.

Note that due to the hardware limitation, e.g., ImpinJ R420 has a phase resolution about 0.0015 radians, the theoretical ranging resolution for COTS RFID readers is

$\frac{3\times10^8\ \mathrm{m\backslash s}}{923\ \mathrm{MHz}} \times \frac{0.0015\ \mathrm{rad}}{4\times\pi\ \mathrm{rad}} = 0.039$ mm [13]. However, it can hardly achieve this precision because of calculation approximation and measurement error.

Different from the existing phase model, this phase model based on polarization effect takes the angle of the label in three dimensions into account, which effectively reduces the error caused by the label angle. As shown in Fig. 1, it is a schematic diagram of antenna placement and coordinate selection in the system. The x-axis parallel to the ground in the X-Y plane of the top antenna is defined as the x-axis of the space, the positive half axis is the horizontal right direction. The y-axis perpendicular to the ground is defined as the Y-axis of the space, the positive half axis is the vertically upward direction. And the axis perpendicular to the X-Y plane is defined as the z-axis, the positive half axis is the direction in which the antenna faces.

In this way, the polarization decomposition vector coordinates of three antennas can be obtained where v vector of all three antennas is (0,1,0), u vector of top antenna A_1 is (1,0,0), u vectors of bottom antennas A_2 and A_3 are $(\frac{\sqrt{2}}{2}, 0, \frac{\sqrt{2}}{2})$ and $(\frac{\sqrt{2}}{2}, 0, -\frac{\sqrt{2}}{2})$. The antenna deployment mode is not unique, as long as the polarization decomposition vector of three antennas can cover three axes in the space. However, in order to reduce the computational complexity and improve the execution efficiency of the system, the above deployment mode is selected in this paper. The number of antennas can also continue to increase. The increase in the number can continue to improve the positioning accuracy, but it will increase the cost. In this paper, three antennas are the minimum requirements for positioning, so three antennas are used in the process of the experiment.

3 Methods

In the previous section, we state the polarization effect and the phase model based on this effect. In this section, we will detail the method about how to calculate the pure phase and how to obtain the measured phase corresponding to the distance.

3.1 Pure phase calculation

In the previous section, theoretical analysis demonstrates that there is no direct linear relationship between the measured phase β, pure phase θ and multipath phase α. In order to simplify the computational complexity, two new variables, multipath variable $\hat{\alpha}$ and mirror phase $\hat{\theta}$, are selected to establish a linear relationship with the measured

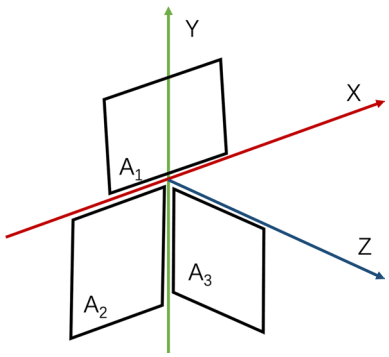

Fig. 1 Schematic diagram of antenna triaxial coordinates

phase β. In this section, we will demonstrate how to utilize the internal relationship under multichannel of the measured phase β to calculate the actual value of the mirror phase $\hat{\theta}$.

First, the measured phase in multichannel β has the following relationship: Assuming that a reader has N channels, the measurement phase β_n under each channel n can be expressed with:

$$\beta_n = \hat{\alpha}_n + \hat{\beta} + (n-1) \cdot \Delta\hat{\theta} \tag{7}$$

where $\hat{\theta}$ is the mirror phase/rad of the first channel; $\hat{\alpha}_n$ is the multipath variable/rad of the nth channel.

The phase change of the signal will change with the change of frequency. Even under the same environmental reflection, the phase at different frequencies is still different. Moreover, path loss and reflection attenuation are also related to frequency. The theoretical path loss in free space is:

$$\text{FSPL (dB)} = 20\log_{10}(d) = 20\log_{10}(f) - 27.55 \tag{8}$$

where d is the path length/M; f is the frequency/Hz.

The reflection attenuation in free space is:

$$\text{RL (dB)} = 20\log_{10}\frac{Z_{in} - Z_0}{Z_{in} + Z_0} \tag{9}$$

where Z_{in} is impedance/Ω and it is frequency dependent.

According to Eqs. (8) and (9), both factors affecting multipath effect will change with frequency. Therefore, multipath variable $\hat{\alpha}_n$ is also different in different channels and varies nonlinearly. However, the phase offset between two adjacent channels $\Delta\hat{\theta}$ varies linearly. It consists of three parts, including the phase difference affected by distance $\Delta\theta_d$, phase difference affected by reader antenna hardware $\Delta\theta_A$ and phase difference affected by tag antenna hardware $\Delta\theta_T$. When the channel changes from n to $n+1$, the wavelength λ will also change, so the received signal will also produce a phase difference affected by the wavelength at the same distance $\Delta\theta_D$. According to the above theoretical equation, the three factors that can impact $\Delta\hat{\theta}$ are all affected by the frequency change. Hence, when the frequency changes linearly in different channels, the phase offset $\Delta\hat{\theta}$ will also vary linearly.

In order to prove the above theory, the following experiments are done in this paper. A label is placed in two environments with open space and dense multipath, and we measure the phase of each of the 16 channels under the conditions of the same distance, the same hardware equipment and the same label angle β_n. As shown in Fig. 2, the phase information measured in the open area is roughly on a straight line, because the multipath impact of the environment in the open area is minor and can be almost ignored, that is $\hat{\alpha}_n \ll \Delta\hat{\theta}$. Therefore, the following expression can be obtained:

$$y' = \kappa' \cdot n + d', \kappa' = \Delta\hat{\theta}, d' = \hat{\theta} - \Delta\hat{\theta} \tag{10}$$

where y' is the ideal fitting line.

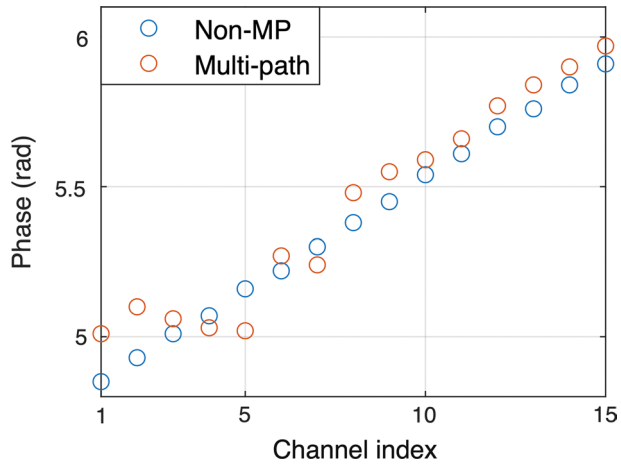

Fig. 2 Phase comparison under different channels

The ideal fitting line can be obtained only when there is no multipath interference, but the phase value measured in the complex actual experimental environment does not necessarily meet the fitting line due to the interference of the multipath effect. Figure 2 shows that in the open environment, the phase and frequency basically conform to the linear relationship, because there are few multipaths in the open environment. In the complex multipath environment, due to the influence of the multipath effect, the measured phase value and frequency do not meet the direct linear relationship. A shake can be observed between channel 3 and channel 8 as well as some small inconsistency along other channels. This is caused by frequency selective fading. It is because, under such complex multipath environments, signals of different central frequencies may travel through different paths causing their propagation distance to vary from channel to channel.

Therefore, the measured phase obtained in the actual experiment is not necessarily accurate, and even there will be large errors. In order to obtain an accurate mirror phase from the measured phase $\hat{\theta}$, quantitative analysis of the measured phase and mirror phase is required, and we can obtain:

$$A \cdot x = b \tag{11}$$

$$x^{T}_{(N+2)\times 1} = [\hat{\alpha}_1, \hat{\alpha}_2, \hat{\alpha}_3, \ldots, \hat{\alpha}_N, \hat{\theta}, \Delta\hat{\theta}] \tag{12}$$

$$b^{T}_{N\times 1} = [\beta_1, \beta_2, \beta_3, \ldots, \beta_N] \tag{13}$$

$$A_{N\times(N+2)} = \begin{bmatrix} 1 & 0 & 0 & \cdots & 0 & 1 & 0 \\ 0 & 1 & 0 & \cdots & 0 & 1 & 1 \\ 0 & 0 & 1 & \cdots & 0 & 1 & 2 \\ \vdots & \vdots & \ddots & \vdots & \vdots & \vdots & \\ 0 & 0 & 0 & \cdots & 0 & 1 & N-1 \end{bmatrix} \tag{14}$$

Obviously, Eq. (11) is a system of non-homogeneous linear equations, in which there are $n+2$ unknowns and n equations, so there are countless solutions of unknowns X. In order to find the effective solution of X, two additional conditions need to be established to fit this set of measurements β_n to a straight line. Hence, an actual fitting line is defined in this paper $y_n = \kappa \cdot n + d$, the purpose of this line is to be as close as possible to the fitting line in the ideal case. Therefore, the difference between the actual fitting line and the ideal fitting line is also defined. The equation is as follows:

$$\phi = \sum_{n=1}^{N} \omega_n \cdot (y_n - \beta_n)^2 \tag{15}$$

where ω_n is the weight of the nth channel.

Because the frequency of each channel is different, the multipath effect of each channel is also different. Therefore, it is necessary to define the channel weight function to reduce the influence of the possible outliers of some channels on the fitting line. The standard of designing channel weight function is very simple, that is, to weaken the influence of the multipath effect as much as possible. The generation of the multipath effect is often composed of two parts, dynamic reflector (such as moving objects and people) and static reflector (such as walls, furniture and ceiling in a room). Compared with the static reflector, the dynamic reflector will produce more uncontrollable and unpredictable errors on the measurement phase, while the static reflector will have a relatively stable error distribution, and the more serious multipath effect will produce more discrete points. Therefore, the purpose of designing the channel weight function is to eliminate the reflection of dynamic multipath as much as possible and estimate the influence of static multipath signal. Therefore, multipath variables can be $\hat{\alpha}_n$ It is divided into two parts, the static multipath component composed of the reflection superposition of the static reflector $\hat{\alpha}_n^s$ And a dynamic multipath component composed of the reflection superposition of the dynamic reflector$\hat{\alpha}_n^d$, i.e.,

$$\sigma_n = \frac{\sum |\beta_n^0 - \overline{\beta_n}|}{t} \tag{16}$$

where β_n^0 is the measurement phase/rad of the nth channel; T is the number of samples; and $overline\beta_n$ is the average value/rad of measured phase under t samples.

After the above analysis, the weight function can be obtained as

$$\omega_n = \frac{N \cdot p_n}{\sum p_n}, \quad n = 1, 2, 3, \ldots, N \tag{17}$$

where p_n is the degree of dispersion of the nth channel for all channels.

Degree of dispersion p_n The measurement equation is:

$$p_n = e^{(\sum_{n=1}^{N} \sigma_n) - (N \cdot \sigma_n)} \tag{18}$$

In order to make the result of the weight function easy to solve and improve the calculation efficiency, the sum of all weight functions ω_n is equal to the number of channels N. Under this calculation method, the influence of the channel affected by the unpredictable and uncontrollable dynamic multipath on the final result is effectively reduced. And

the dynamic multipath effect generally obeys Gaussian distribution, so it can be considered as $\sum_{n=1}^{N} \omega_n \cdot \hat{\alpha}_n^d$ when the number of samples is large enough. This weight function can be used to obtain more accurate fitting results.

As Eq. (15) suggests, when the error ϕ gets its minimum, the slope κ and intercept d closest to the ideal fitting line can be obtained. Therefore, by demanding ϕ on the slope κ and intercept d partial derivatives, we can obtain:

$$\begin{cases} \kappa = \Delta\hat{\theta} + e_1, e_1 = \dfrac{N \cdot \sum \omega \cdot n \cdot \hat{\alpha}_n - \sum \omega \cdot n \sum \omega \cdot \hat{\alpha}_n}{N \cdot \sum \omega \cdot n^2 - (\sum \omega \cdot n)^2} \\ d = \hat{\theta} - \Delta\hat{\theta} + e_2, e_2 = \dfrac{\sum \omega \cdot n^2 \cdot \sum \omega \cdot \hat{\alpha}_n - \sum \omega \cdot n \cdot \hat{\alpha}_n \cdot \sum \omega \cdot n}{N \cdot \sum \omega \cdot n^2 (\sum \omega \cdot n)^2} \end{cases} \tag{19}$$

where e_1 is the difference of slope between the fitting line and the ideal line; e_2 is the difference of intercept between the fitted line and the ideal line. After that, we leverage linear regression (LR) to estimate the original phase. Although the phase error does not follow the Gaussian distribution, we can feel comfortable using ordinary least squares (OLS) since Gaussian–Markov theorem (GMT) [14] guarantees it is the best linear unbiased estimator (BLUE) in this case. The GMT states that the OLS estimator has the lowest sampling variance within the class of linear unbiased estimators, if the errors in the linear regression model are uncorrelated and have equal variances and expectation value of zero. We know that the measurement errors are independent. The mean residual of phase error is about 10^{-7}. The residual can pass the Breusch–Pagan test, which means equal variances. As shown in Fig. 3, the LR line, which uses OLS, and the LAR line, which uses the least absolute residual solution for robust estimation, almost perfectly coincide. Hence, we leverage OLS to estimate the phase for convenience.

In this system, the calculated tag angle is used to obtain the phase model based on the polarization effect on the three antennas. Then the measured phase actually received is phase decomposed and pure phase calculated. The multipath information in the environment is eliminated, and finally, the distance is calculated by using the phase difference at different frequencies.

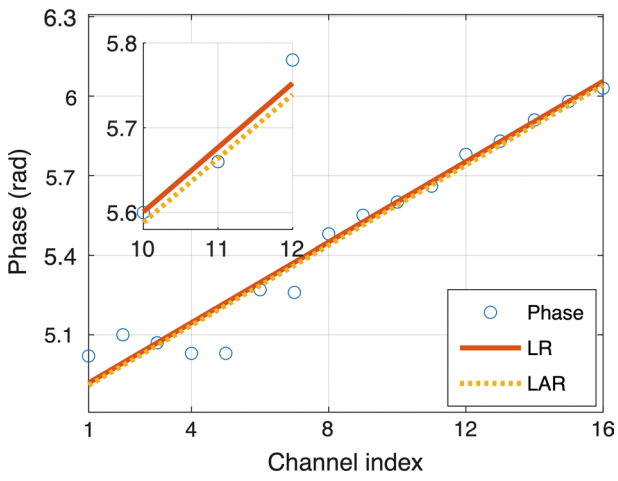

Fig. 3 Fitting effect

3.2 Phase unwrapping

In the RFID system, the measured phase value received by the reader is actually a roll phase, that is:

$$\theta_{\text{true}} = \theta + 2k\pi, \quad k = 1, 2, \ldots, n \tag{20}$$

where θ_{true} is the true phase/rad; θ is the measured phase/rad. The difference between the true phase and the measured phase is going to be $k \times 2\pi$. Therefore, if the measured phase is directly used for positioning, the effective positioning distance does not exceed half wavelength, about 16 cm, which is far less than the distance requirements of general positioning. So, the calculation of k is required. This process is called phase unwrapping, also known as integer ambiguity resolution. In this paper, HMFCW algorithm is used to solve the integer ambiguity. [7]

As shown in Fig. 4, the schematic diagram of HMFCW is provided. Under the n different frequency, we sample the phase of the same tag. Ideally, the theoretical distance between the tag and the reader antenna is:

$$d_i = d_h + d_m = k_i \times \lambda_i + \frac{\theta_i}{2\pi} \times \lambda_i, \quad i = 1, 2, \ldots, n \tag{21}$$

where i is the first i frequency; d_h is the integer wavelength distance calculated from integer cycles/M; d_m is the distance calculated from measured phase/M; k_i is the first i integer ambiguity at two frequencies; λ_i is the first i wavelength at two frequencies/M; and θ_i is the first i measured phase/rad at two frequencies.

The overall idea of HMFCW is getting n measurement of phase under n different frequency and calculating the distance corresponding to each phase measurement as $\frac{\theta_i}{2\pi} \times \lambda_i$. Then adding 0, 1, 2...$N$ wavelengths, respectively, to obtain $n + 1$ distance values. Because the real distance is fixed, the values with similar distances obtained at different frequencies can be grouped into a cluster, and the group with the best clustering result can be selected as the ranging result, so as to realize positioning. However, the phase obtained in the actual scene often has a certain error, so it is necessary to have a certain error tolerance for the phase, and the phase tolerance is proposed $\Delta\theta_i$; the theoretical distance in the real scene can be expressed as:

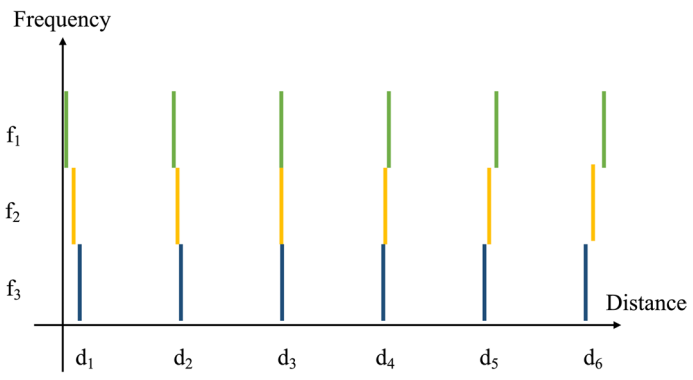

Fig. 4 Schematic diagram of HMFCW

$$d_i = d + \frac{\theta_i}{2\pi} \times \lambda_i \tag{22}$$

where d is the true distance/M and $\Delta\theta_i$ is the frequency Phase tolerance under f_i. It is assumed that the absolute value of phase tolerance at all frequencies is less than an upper limit tolerance $\Delta\theta_{\max}$; then, subtract the theoretical distance at the two frequencies to obtain:

$$|d_i - d_j| = \left| n_i \times \lambda_i + \frac{\theta_i}{2\pi} \times \lambda_i \times \lambda_i - n_j \times \lambda_j - \frac{\theta_j}{2\pi} \times \lambda_j \times \lambda_j \right| < \frac{\Delta\theta_{\max}}{2\pi} \times (\lambda_i + \lambda_j) \tag{23}$$

where n_i is the number of full cycles at ith frequency and n_j is the number of full cycles at jth frequency.

According to Eq. (23), if $\Delta\theta_{\max}$ is too large, there will be multiple clusters of whole weeks that meet the filtering criteria. Therefore, if you want to have a unique solution to Eq. (23), you need to limit $\Delta\theta_{\max}$ as follows:

$$\Delta\theta_{\max} = \frac{\pi \times (f_{\max} - f_{\min})}{f_{\max} + f_{\min}} \tag{24}$$

where $f_{\max}$ is the maximum frequency of frequency conversion signal/MHz and $f_{\min}$ is the minimum frequency of frequency conversion signal/MHz.

Equation (24) shows the relationship between phase tolerance and frequency. The distance between two frequencies can be obtained by making a difference:

$$\begin{cases} 2\pi \times \dfrac{\left| n_i \times \lambda_i + \frac{\Delta\theta_i}{2\pi} \times \lambda_i - n_j \times \lambda_j - \frac{\Delta\theta_j}{2\pi} \times \lambda_j \right|}{\lambda_i + \lambda_j} < \Delta\theta_{\max} \\ n_i \le \dfrac{R_{\max}}{\lambda_i}, i = 1, 2, \ldots, N \end{cases} \tag{25}$$

where $R_{\max}$ is the maximum ranging range/m.

Equation (25) shows that when the measurement phase error at all frequencies is less than $\Delta\theta_{\max}$, there must be a unique whole cycle solution, and then, the positioning result is calculated. However, in the actual measurement, the phase error may still be greater than the phase tolerance. At this time, it is necessary to slowly expand the phase tolerance to ensure that there is a unique whole cycle cluster to meet the conditions.

The size of phase error is an important index affecting the accuracy of HMFCW algorithm. Once some frequencies are greatly offset under the influence of complex multipath environments, it will directly have a great impact on the positioning results. Therefore, it is necessary to study the impact of different sizes of phase error on ranging accuracy.

Suppose there are two frequencies f_i and f_j, the wavelengths corresponding to these two frequencies are λ_i and λ_j, and $f_i < f_j$, $\lambda_i > \lambda_j$. Denote the corresponding phase errors as $-\Delta\theta_{\max}$ and $\Delta\theta_{\max}$. Therefore, the distances calculated by these two frequencies can be subtracted and get:

$$2\pi \times \frac{-\frac{\Delta\theta_{\max}\times\lambda_i}{2\pi} \times \lambda_i - \frac{\Delta\theta_{\max}\times\lambda_j}{2\pi} \times \lambda_j}{\lambda_i + \lambda_j} = \frac{-\pi \times (f_{\max} - f_{\min})}{f_{\max} + f_{\min}} \tag{26}$$

Equation (26) shows that when the phase error is $\Delta\theta_{\max}$. It is also the phase tolerance, and there must be a unique solution for the whole cycle. So when the phase error is less than $\Delta\theta_{\max}$, a unique solution must exist. When the whole cycle number cluster needs to be solved for positioning, the whole cycle number of the similar distance at each other frequency needs to be calculated based on the distance corresponding to the maximum frequency. Let the maximum frequency be $f_{\max}$. The wavelength at this frequency is $\lambda_{\min}$. The corresponding phase error at the maximum frequency is $\Delta\theta_{\max}$. The corresponding number of whole cycles at frequency f_i is:

$$\frac{\frac{\Delta\theta_{\max}}{2\pi} \times \lambda_i - \frac{-\Delta\theta_{\max}}{2\pi} \times \lambda_{\min} + r \times \lambda_{\min}}{\lambda_i} = \frac{f_{\max} - f_{\min}}{2(f_{\max} + f_{\min})}\left(1 + \frac{f_i}{f_{\max}}\right) + r\frac{f_i}{f_{\max}} \tag{27}$$

where r is the whole cycle difference count between f_i and $f_{\max}$.

Because the number of whole cycles at different frequencies will be different, r needs to be calculated. The calculation equation is:

$$round\left(\frac{f_{\max} - f_{\min}}{2(f_{\max} + f_{\min})}\left(1 + \frac{f_i}{f_{\max}}\right) + r\frac{f_i}{f_{\max}}\right) = r \tag{28}$$

where *round* is the rounding function.

The real distance between the antenna and the tag can be obtained after the above integer cycle processing. The whole steps of the positioning algorithm based on pure phase extraction are summarized as shown in Algorithm 1:

Algorithm 1: Positioning algorithm

Input: ϑ_i, $(i = 1, 2, \cdots, 16)$ /* phase angle under 16 different frequencies. */
Output: D /* The distance between the tag and the target. */
Decompose ϑ_i and obtain pure phase θ_i using Equation (15);
Calculate max phase offset $\Delta\theta_{max}$ using Equation (24);
for *True* **do**
  Calculate candidate distance d_{candi} using Equation (21);
  Cluster d_{candi} with distance ($\Delta\theta_{max}$) among different frequencies, and obtain the corresponding number of whole cycles n_i using Equation (28);
  if n_i *makes Equation* (25) *hold* **then**
    break;
  else
    $\Delta\theta_{max} \leftarrow \Delta\theta_{max} \times 1.01$;
  end
end
Calculate Distance $D = \frac{1}{16}\sum_{i=1}^{16}\left(\left(n_i + \frac{\theta_i}{2\pi}\right) \times \lambda_i\right)$;

4 Results and discussion

In this section, the above methods are tested in different scenarios, and the experimental results are used to evaluate the system.

4.1 Environmental configuration

This paper mainly studies the three-dimensional positioning of RFID tags in indoor scenes. The system is mainly composed of an Impinj RFID reader and three corresponding matched circular polarization antennas Laird s9028pcr. As shown in Fig. 5, we conduct our experiments in three different scenarios: (a) outdoor case, (b) indoor case with weak multipath effect and (c) indoor case with strong multipath effect. For each experiment, we utilize three antennas and one tag. The tag is positioned on a test stand with rotation functionality. Three antennas are positioned as one on the top and two at the bottom. The bottom two antennas are horizontally placed with an angle of 90 degrees. And the entire antenna setup is facing toward the tag. We locate 10 kinds of RFID tags in the space of $2 \times 2 \times 2\,\mathrm{M}^3$. The reader Impinj r420 follows EPC global C1G2 protocol and operates at 920.625–924.375 mhz with 16 channels in total. The bandwidth of the each channel is 231.25 kHz, and the transmission power of the directional antenna is set to 30 dBm by default.

4.2 Impact of different environments

In the practical application of the RFID system, the real scene must be far from the laboratory environment. In the actual environment, the system will face a variety of environmental conditions, but the difference in environmental conditions is actually attributed to the difference of multipath. Therefore, in order to evaluate the positioning effect under different multipath conditions, this paper selects three representative environments with typical real application conditions as the test, namely outdoor open environment, indoor weak multipath environment and indoor strong multipath environment.

In this paper, the system is arranged in these three environments, respectively, and the control variable method is adopted to only change the environment to ensure that all other parameters in the system except distance are exactly the same. The aln-9640 tag carrying m730 chip was used as the positioning target in the experiment $\times 2\times$ Select several positions within 1m for positioning test, collect data for 3 times at each position, and calculate the distance error of each collected data, respectively, $\Delta d(i)$ Finally, the distance error of each position is recorded as: $\Delta = \sum_{i=1}^{3} \Delta d(i)/3$.

As shown in Fig. 6, it can be seen from experience that the positioning errors are often different in different environments. The more complex the environment is, the richer the multipath information is, and the greater the interference to the RF signal is. The same is the experimental result. In the outdoor open environment, only the tag itself and the

(a) Outdoor (b) Indoor Weak Multipath (c) Indoor Strong Multipath

Fig. 5 Experiments scenario

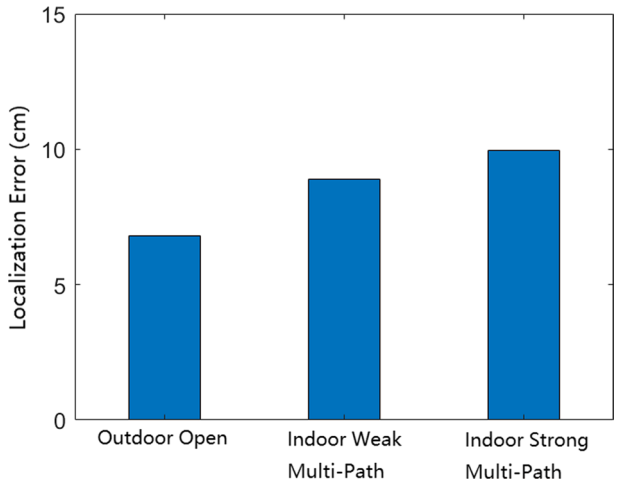

Fig. 6 Positioning error under different environments

ground can reflect the RF signal, and the multipath information is the least, so the positioning error is the smallest, with an error of 6.79 cm. The indoor weak multipath environment contains labels, ground, walls and a small number of other objects, which has more multipath information than the outdoor open environment. Therefore, the positioning error is higher than the outdoor open environment, with an error of 8.90 cm. In the indoor strong multipath environment, many reflectors are added on the basis of the indoor weak multipath environment to simulate the warehouse placement in the real scene. A large number of items are often stacked in the real warehouse, and the number of reflectors is countless, which often has strong multipath information. Therefore, the error is the largest among the three environments, with an error of 9.90 cm. The errors in the three environments are less than half the wavelength of the RF signal. Within the expected positioning error range, it is proved that the system is feasible in a variety of environments.

4.3 Impact of dynamic multipath

In the real scene, there cannot be only static multipath information in the environment near the label to be located, and the uncertainty and unpredictability of dynamic multipath information are often the biggest factors causing errors.

In order to simulate the real environment, in this experiment, a person walks around the label to be tested irregularly to simulate the dynamic multipath information in the real environment, and tests are carried out in the three environments in the previous section. The results are shown in Fig. 7. Under the three environments, the positioning error with dynamic multipath information in the environment to be tested is greater than that without dynamic multipath information, in which in the outdoor open environment, the positioning error with dynamic multipath information is 8.39 cm, which is 23.41% higher than that without dynamic multipath information. The positioning error with dynamic multipath information in an indoor weak multipath environment is 12.28 cm, which is 46.72% higher than that without dynamic multipath information. The positioning error with dynamic multipath information in indoor strong multipath

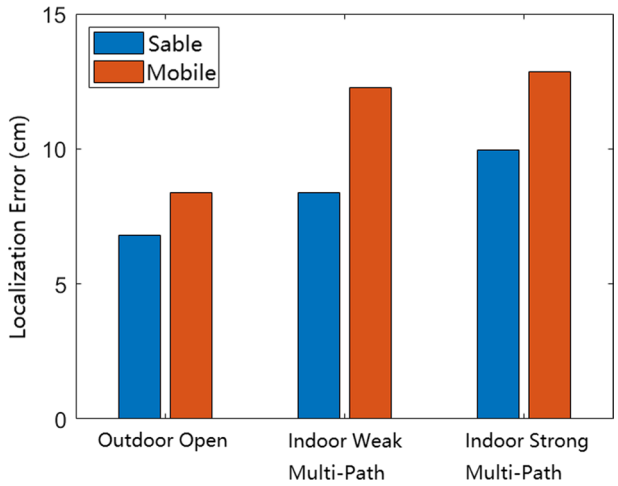

Fig. 7 Positioning error with moving object

environment is 12.86 cm, which is 29.22% higher than that without dynamic multipath information.

The above experimental results show that in an open environment, even if there is dynamic multipath information, the impact of dynamic multipath on the positioning will not increase significantly due to the small number of reflectors. In the more complex indoor environment, due to the large number of reflectors, once the dynamic multipath information is added, the effect of affecting the positioning accuracy will increase significantly. However, when the number of reflectors reaches a certain extent, a small amount of dynamic multipath will affect the positioning accuracy, but the impact will not be particularly large.

4.4 Impacts of different distances

In order to verify the influence of the positioning distance on the algorithm and ensure a good positioning effect in the measurement range, we conducted experiments using the control variable method.

This experiment only changes the distance between the tag and the antenna under the experimental conditions of the fixed experimental environment and tag type. And the distance is distributed between 20 cm and 200 cm. In the experiment, every 20 cm is divided as an interval, 20 samples are measured in each interval, and the positioning error of each sample is calculated. As shown in Fig. 8, the positioning error at all distances is below half wavelength, the minimum average error is 6.96 cm, and the maximum average error is 12.41 cm. With the increase in the distance, the positioning error has a certain positive correlation, but more than 70% of the positioning error is concentrated in 8–12 cm, and the maximum positioning error is only 16.15 cm. Within the range of expected positioning error, it shows that the work has high positioning accuracy within the existing agreed range.

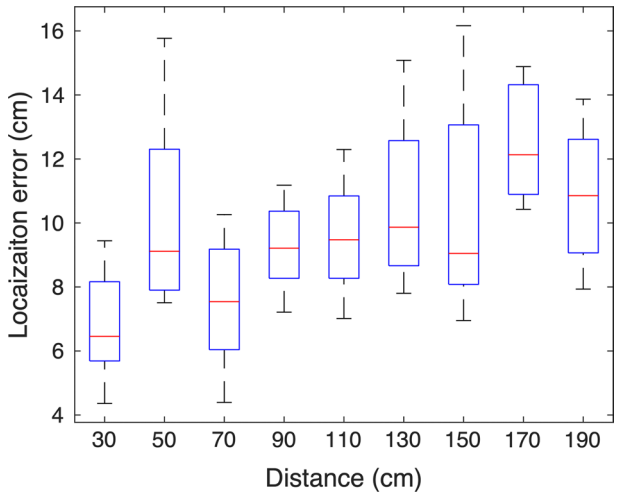

Fig. 8 Positioning error at different distances

Table 1 Comparisons with existing algorithm

Solution	Antenna array	Mobile antenna	Pre-training	Mean error (cm)
3DinSAR [7]	N	Y	Y	24.30
3DTagArray [15]	Y	N	N	9.00
Phase Relock [16]	N	Y	N	54.86
RF-MVO [17]	N	Y	N	6.23
3DLRA [18]	Y	N	Y	10.02
Ours	N	N	N	8.90

4.5 Comparison with existing algorithms

In order to illustrate the availability and reliability of our solution, as shown in Table 1, we compare some existing works, including 3DinSAR, 3DTagArray, Phase Relock, RF-MVO and 3DLRA. These works are only tested in a single environment. In order to reduce the comparison error, this paper selects the indoor weak multipath environment scene as the work comparison. Among them, 3DinSAR uses the principle of interferometric synthetic aperture radar (InSAR) to simulate a multiantenna array by moving antenna in the plane to achieve the purpose of positioning. Compared with the method in this paper, 3DinSAR has the problems of large error and inconvenient deployment. 3DTagArray adds energy collection circuit and motion sensor on the commercial label and binds 2-4 label arrays on the object to locate the target. Although it has good positioning effect, the transformation of the label undoubtedly increases the cost of deployment and the difficulty of popularization. Phase Relock binds a single antenna to the robot and simulates the antenna array through the movement of the robot. Compared with 3DinSAR algorithm, it has lower computational complexity and higher real-time performance, but at the same time, the error also increases significantly, which is not a suitable positioning choice. RF-MVO combines RF signal positioning with monocular camera. By installing monocular camera on the mobile antenna, the phase and received signal strength of the tag are

measured through the antenna in the process of moving, and the visual information is captured by the monocular camera to improve the positioning accuracy. Although it can have high positioning accuracy, the positioning cost is also the highest. 3DLRA uses deep learning to input the phase, received signal strength and time stamp as features into the convolutional neural network (CNN) for positioning. Although it has high positioning accuracy, the method based on deep learning often requires a long training time and is strongly dependent on the environment. Once the environment is changed, it needs to be retrained, and the portability is poor. The three-dimensional positioning algorithm proposed in this paper has a good positioning effect in various environments and does not need additional hardware. All system deployment is completely carried out on the basis of existing commercial equipment and has good environmental adaptability and portability.

However, we should point out that our solution can achieve 3D localization for the stable object. Nevertheless, due to the Doppler frequency shift, the proposed solution cannot track moving objects.

5 Conclusion

In this paper, we propose a 3D localization system for RFID. The main work and innovations of this paper are summarized as follows: (1) A phase model based on the polarization effect is proposed to make up for the influence of the phase error caused by ignoring the label angle in the existing phase model, and the phase accuracy is improved by phase unwrapping and phase filtering based on discrete wavelet transform. (2) By analyzing the vector relationship between the received phase, the pure phase and the multipath variable, a positioning algorithm based on the pure phase extraction is proposed, which removes the multipath variable from the received phase, solves the problem that the error of the traditional positioning method increases significantly in the multipath environment, and uses the HMFCW algorithm to unwrap the phase and recover the real phase information. (3) There is no need to refer to labels or anchors, nor to collect training data, which greatly enhances the environmental portability of the method. Using commercial RFID equipment, a

Table 2 Abbreviations table

Technical term	Abbreviation
Radio frequency identification	RFID
Heuristic multifrequency continuous wave	HMFCW
Ultra-high frequency	UHF
Radio frequency	RF
Global positioning system	GPS
Ultra-wideband	UWB
Linear regression	LR
Line of sight	LOS
Interferometric synthetic aperture radar	InSAR
Convolutional neural network	CNN

three-dimensional positioning algorithm with easy deployment, high precision and low cost is realized, and the average positioning error is about 9 cm.

6 Abbreviations

The technical terms we used in this manuscript are list in the glossary, as shown in Table 2.

Author's contributions
W.S. proposed the basic idea and analyzed the polarized features of the phase. K.Z. and Z.C. leveraged HMFCW to unwrap the polarized phase. Z.G. analyzed and verified that the OLS was appreciated to fit the phase data. Y.Q., P.W. and et al. performed the experiments. All authors read and approved the final manuscript.

Funding
This work is supported by the Natural Science Foundation of China under Grants. 61802299, 62002284, and the Fundamental Research Funds for the Central Universities xzy012020019.

Availability of data and materials
Some of the raw data is available on the Github website, "https://github.com/pandazhao/Target-Localizaiton.git." Please contact the author for more data.

Declarations

Competing interests
The authors declare that they have no competing interests.

Author details
[1]School of Computer Science and Technology, Xi'an Jiaotong University, Xi'an, China. [2]Xlab, The Second Academy of China Aerospace Science and Industry Corp, Beijing, China.

Received: 25 October 2021 Accepted: 2 March 2022
Published online: 16 March 2022

References

1. Y. Yin, Q. Huang, H. Gao, Y. Xu, Personalized APIs recommendation with cognitive knowledge mining for industrial systems. IEEE Trans. Ind. Inf. **17**(9), 6153–6161 (2020)
2. H. Gao, L. Zhou, J.Y. Kim, Y. Li, W. Huang, Applying probabilistic model checking to the behavior guidance and abnormality detection for mci patients under wireless sensor network. ACM Trans. Sensor Netw. (2021). https://doi.org/10.1145/3499426
3. H. Gao, C. Liu, Y. Yin, Y. Xu, Y. Li. A hybrid approach to trust node assessment and management for VANETs cooperative data communication: historical interaction perspective. IEEE Trans. Intell. Transp. Syst. pp. 1–10 (2021)
4. Y. Yin, Z. Cao, Y. Xu, H. Gao, R. Li, Z. Mai, Qos prediction for service recommendation with features learning in mobile edge computing environment. IEEE Trans. Cogn. Commun. Netw. **6**(4), 1136–1145 (2020)
5. X. Ma, H. Xu, H. Gao, M. Bian, Real-time multiple-workflow scheduling in cloud environments. IEEE Trans. Netw. Serv. Manag. **18**(4), 4002–4018 (2021)
6. A.S. Paul, E.A. Wan, Rssi-based indoor localization and tracking using sigma-point Kalman smoothers. IEEE J. Sel. Top. Signal Process. **3**(5), 860–873 (2009). https://doi.org/10.1109/JSTSP.2009.2032309
7. Y. Ma, X. Hui, E.C. Kan, 3d real-time indoor localization via broadband nonlinear backscatter in passive devices with centimeter precision, in *Proceedings of the 22nd Annual International Conference on Mobile Computing and Networking, MobiCom 2016, New York City, NY, USA, October 3–7, 2016*. ed. by Y. Chen, M. Gruteser, Y.C. Hu, K. Sundaresan (ACM, 2016), pp. 216–229. https://doi.org/10.1145/2973750.2973754
8. M. Vari, D. Cassioli, mmwaves RSSI indoor network localization, in *IEEE International Conference on Communications, ICC 2014, Sydney, Australia, June 10–14, 2014, Workshops Proceedings* (IEEE, 2014), pp. 127–132. https://doi.org/10.1109/ICCW.2014.6881184
9. B. Zhou, A. Liu, V.K.N. Lau, Successive localization and beamforming in 5g mmwave MIMO communication systems. IEEE Trans. Signal Process. **67**(6), 1620–1635 (2019). https://doi.org/10.1109/TSP.2019.2894789
10. S.M. Djosic, I.Z. Stojanovic, M.D. Jovanovic, T.R. Nikolic, G.L. Djordjevic, Fingerprinting-assisted uwb-based localization technique for complex indoor environments. Expert Syst. Appl. **167**, 114188 (2021). https://doi.org/10.1016/j.eswa.2020.114188
11. L. Li, K. Yang, X. Bian, Q. Liu, Y. Yang, F. Ma, A gas leakage localization method based on a virtual ultrasonic sensor array. Sensors **19**(14), 3152 (2019). https://doi.org/10.3390/s19143152
12. S. Haigh, J. Kulon, A. Partlow, P. Rogers, C. Gibson, Improved obstacle mitigation and localization accuracy in narrowband ultrasonic localization systems using Robcul algorithm. IEEE Trans. Instrum. Meas. **69**(5), 2315–2324 (2020). https://doi.org/10.1109/TIM.2019.2963553

13. L. Yang, Y. Chen, X.-Y. Li, C. Xiao, M. Li, Y. Liu. Tagoram: real-time tracking of mobile RFID tags to high precision using cots devices, in *Proceedings of the 20th Annual International Conference on Mobile Computing and Networking* (2014), pp. 237–248
14. C.E. Heckler, *Applied Multivariate Statistical Analysis* (Taylor & Francis, Boca Raton, 2005)
15. L. Qiu, Z. Huang, N. Wirström, T. Voigt. 3dinsar: object 3d localization for indoor RFID applications, in *2016 IEEE International Conference on RFID, RFID 2016, Orlando, FL, USA, May 3–5, 2016* (IEEE, 2016), pp. 191–198. https://doi.org/10.1109/RFID.2016.7488026
16. A. Tzitzis, S. Megalou, S. Siachalou, E.G. Tsardoulias, T.V. Yioultsis, A.G. Dimitriou. 3d localization of RFID tags with a single antenna by a moving robot and "phase relock", in *IEEE International Conference on RFID Technology and Applications, RFID-TA 2019, Pisa, Italy, September 25-27, 2019* (IEEE, 2019), pp. 273–278. https://doi.org/10.1109/RFID-TA.2019.8892256
17. S. Cheng, S. Wang, W. Guan, H. Xu, P. Li, 3dlra: an RFID 3d indoor localization method based on deep learning. Sensors **20**(9), 2731 (2020). https://doi.org/10.3390/s20092731
18. Z. Wang, M. Xu, N. Ye, F. Xiao, R. Wang, H. Huang, Computer vision-assisted 3d object localization via COTS RFID devices and a monocular camera. IEEE Trans. Mob. Comput. **20**(3), 893–908 (2021). https://doi.org/10.1109/TMC.2019.2954830